Charge-carrier density independent mobility in amorphous fluorene-triarylamine copolymers

Alasdair J. Campbell*, Ruth Rawcliffe, Alexander Guite, Jorge Costa Dantas Faria, Abhimanyu Mukherjee, Martyn McLachlan, Maxim Shkunov, and Donal D. C. Bradley

[*] Dr R. Rawcliffe, Dr A. Guite, J. Costa Dantas Faria, A. Mukherjee, Prof. D. D. C. Bradley and Dr A. J. Campbell
Department of Physics and the Centre for Plastic Electronics, Imperial College London, Blackett Laboratory, South Kensington campus, London SW7 2AZ, UK

Dr M. McLachlan
Department of Material Science and the Centre for Plastic Electronics, Imperial College London, South Kensington campus, London SW7 2AZ, UK

Dr Maxim Shkunov
Advanced Technology Institute, Electronic and Electrical Engineering, University of Surrey, Guildford, Surrey, GU2 7HX, UK

Current address: Prof. D. D. C. Bradley, University of Oxford, 9 Parks Road, Oxford, OX1 3PD, UK

Email: alasdair.campbell@imperial.ac.uk

Abstract
A charge-carrier density dependent mobility has been predicted for amorphous, glassy energetically-disordered semiconducting polymers, which would have considerable impact on their performance in devices. However, previous observations of a density dependent mobility are complicated by the polycrystalline materials studied. Here we investigate charge transport in field-effect transistors and diodes of two amorphous, glassy fluorene-triarylamine copolymers, and explore the results in terms of a charge-carrier density dependent mobility model. The non-dispersive nature of the time-of-flight (TOF) transients and analysis of dark injection transient results and transistor transfer characteristics indicate a charge-carrier density independent mobility in both the low-density diode and the high-density transistor regimes. The mobility values for optimised transistors are in good agreement with the TOF values at the same field, and both have the same temperature dependency. The measured transistor mobility falls two to three orders of magnitude below that predicted from the charge-carrier density dependent model, and does not follow the expected power-law relationship. The experimental results for these two amorphous polymers are therefore consistent with a charge-carrier density independent mobility, and we discuss this in terms of polaron-dominated hopping and interchain correlated disorder.

Keywords: organic semiconductor, semiconducting polymer, amorphous polymer, mobility, charge transport, energetic disorder, field-effect transistor, diode

Introduction

Organic semiconductors (OSCs) such as conjugated polymers can be used in a range of different optoelectronic devices, including organic light emitting diodes (OLEDs), organic photovoltaics (OPVs) and organic field-effect transistors (OFETs). A crucial parameter in the development of these technologies is the OSC charge-carrier mobility, and how it is related to the different OSC materials, processing, device architectures and device operating conditions. Many semiconducting polymers and small molecules are amorphous, and such disorder in the physical morphology is expected to reflect itself in disorder of the energy levels of the hole and electron transport states (Figure 1a). Such energetic disorder will directly impact charge transport and mobility [1-12].

For such energetically disordered OSCs, one feature predicted by many charge transport models is a charge-carrier density dependent mobility. The original Gaussian disorder model (GDM) developed by Bässler for

hopping transport in a Gaussian density of states (DOS) distribution was a single carrier approach [1], as were the models based on it which considered both correlated energetic disorder [2], with a smoothly varying energy landscape (see Figure 1a), and the effect of polaronic relaxation [3]. The percolation model developed by Vissenberg and Matters for transport involving an exponential DOS instead considered multiple carriers [4], and this predicted a mobility which has a power-law dependency on the charge-carrier density [5]. Multiple carriers have additionally been included for various models involving a Gaussian DOS, such as the effective-median approximation theory [6], the extended GDM (EGDM) [7], and a recent scaling theory percolation model [8]. These again predict a mobility which increases with increasing charge-carrier density, additionally showing that the temperature dependency of charge transport should simultaneously decrease [9], and that correlated energetic disorder and polaronic effects will vary the behaviour [6, 8, 10-12].

Experimentally, OFETs probe the high charge-carrier density regime between about 10^{17} and 10^{20} cm^{-3}, whilst diodes (OPVs and OLEDs) probe the low charge-carrier density between about 10^{15} to 10^{17} cm^{-3}. The total number of transport states (based on the molecular or conjugation length density) is about 5×10^{20} cm^{-3}, so in OFETs there is about 1 carrier per 10 to 100 sites, while in diodes there is about 1 carrier per 10,000 to 100,000 sites. Tanase *et al* have investigated the charge-carrier density dependence of the mobility in poly(3-hexylthiophene) (P3HT) and different soluble poly(phenylene-vinylene) (PPV) copolymers in both OFETs and in diodes, the latter using steady-state space charge limited current (SCLC) measurements [5, 13]. The OFET results in the high-density regime could be fitted to the power-law dependency of mobility with carrier density predicted by Vissenberg and Matters, and successfully linked to both the magnitude and Gaussian DOS width of the SCLC diode mobility in the low-density regime. Results for MEH-PPV OFETs and diodes indicate a power law dependency extended across both regimes from 10^{15} to 10^{20} cm^{-3} [14]. OFET measurements for pentacene and C60 in the high-density regime also indicate a mobility whose magnitude and temperature dependence vary with charge-carrier density [9]. Transient mobility measurements of P3HT and poly(2,1,3-benzothiadiazole-4,7-diyl[4,4-bis(2-ethylhexyl)-4H-cyclopenta[2,1-b:3,4-b']dithiophene-2,6,diyl]) (PCPDTBT) in solar cells also indicate a charge-carrier density dependent mobility in the low-density regime from 2×10^{16} to 3×10^{17} cm^{-3} [15].

However, there is an intriguing discontinuity between the material systems envisaged by the models, and some of the above material systems used to test them.

The models have been developed for amorphous, glassy materials in which the energy landscape is either uncorrelated or correlated and forms a Gaussian or exponential DOS (see Figure 1a). In contrast, P3HT is polycrystalline, consisting of small crystals (aggregates) embedded in an amorphous fraction [16-18], and the diode mobility varies with film thickness as the morphology changes [19]. MEH-PPV films consists of ordered nanoscale domains (aggregates) embedded in amorphous material, diode mobility varying with film morphology [20-23]. PCPDTBT films again consist of polycrystalline domains embedded in amorphous material [24]. Pentacene and C60 form pure polycrystalline thin films [25, 26]. The energy landscape and DOS for such polycrystalline-amorphous blend systems and polycrystalline systems would be expected to differ considerably from that of a pure amorphous glass (see Figure 1b and c). Even at low crystalline fractions charge transport is expected to deviate from that in a pure amorphous system, the crystals or aggregates acting as deep charge traps. At high crystalline fractions, transport will tend towards the pure polycrystalline materials, where tunnelling between crystals and grain boundary charge trapping dominate. In such materials one is entering a regime where mobility-edge models become much more physically reasonable [27-30].

To really test transport models based on amorphous materials therefore requires the use of amorphous, glassy organic semiconductors. Fluorene-triarylamine copolymers are specifically designed to be amorphous, with high glass transition temperatures, for use as interlayer and hole transport layer materials in polymer light emitting diodes [31-37]. They have also been used, along with the homopolymer poly(triarylamine) (PTAA), as p-type semiconductors in OFETs, allowing highly uniform charge transport over large-area substrates, an important requirement for applications such as display backplanes [38]. Their charge transport has been extensively studied in bulk diodes using the time-of-flight (TOF) and transient SCLC dark injection techniques [39-42], and modelled in the low-charge carrier density regime using the GDM, correlated GDM and polaronic correlated GDM [43]. More recently they have also been used to test the correlated and uncorrelated EGDM in the low charge-carrier density regime using steady-state SCLC diode measurements [44].

Here we investigate the charge-density dependence of the hole mobility across both the low- and high-charge carrier density regimes in two fluorene-triarylamine copolymers, poly(9,9–dioctylfluorene-*co*-bis-*N,N'*-(4-butylphenyl)-bis-*N,N'*-phenyl-1,4-phenylenediamine) (PFB) and poly(9,9–dioctylfluorene-*co*-bis-*N,N'*-(4-methoxyphenyl)-bis-*N,N'*-phenyl-1,4-phenylenediamine) (PFMO). These have been chosen due to their low ionization potentials to minimize the impact of any charge injection effects on the measured mobility values. TOF

measurements and analysis of literature transient SCLC dark injection results are used to investigate hole transport in the low-density diode regime, while OFET measurements are used to investigate the high-density transistor regime. The power-law dependency of the transistor mobility is calculated for the Vissenberg and Matters model from the TOF Gaussian DOS width, and compared to the measured OFET values. The temperature variation of the mobility from TOF and OFETs were additionally compared. Fascinatingly, the results indicate that hole transport in PFB and PFMO is charge-carrier density independent, the best performing transistors having mobility values equal to the diodes at the same field value despite the large differences in carrier density. We discuss the implications of these results in terms of charge transport in amorphous and polycrystalline organic semiconducting materials.

Results and discussion

We first explored the physical morphology of thin films of PFB and PFMO (chemical structure Figure 2a). Differentially scanning calorimetry (DSC) spectra (Figure 2b) are relatively featureless, showing a single broad, weak peak upon heating and cooling, which can be associated with the second-order glass transition temperature. These are very similar to that for TFB [36], and other fluorene-triarylamine copolymers are also found to only exhibit this second-order glass transition [38, 45]. This is very different from that of polycrystalline polymers such as P3HT, poly(9,9-dioctylfluorene) (PFO), poly(9,9-dioctylfluorene-*alt*-benzothiadiazole) (F8BT) and poly(9,9-dioctylfluorene-*alt*-bithiophene) (F8T2), which can have rich and complex DSC spectra showing multiple peaks from glass, crystallization and melting transitions [36, 46-51]. The thin film optical absorption spectra of PFB and PFMO (Figure 2c) are broad and featureless, and strongly resemble the solution spectra using a good solvent in which the chains are in the random-coil conformation. This is exactly as for TFB, being an expected characteristic of an amorphous semiconducting polymer [36]. Polycrystalline polymers such as P3HT, F8BT and PFO instead typically show a red shift of the absorption edge and/or more structure with vibrational sideband detail in their thin film spectra compared to the good-solvent solution spectra [17, 36, 47, 48, 52-54]. We additionally recorded the X-ray diffraction (XRD) spectrum (Supplementary Information (SI) Figure S1) of a 330nm thick film of PFB annealed for 1 hour at 150° C just above the glass transition temperature to encourage any potential crystallite formation (PFMO was not investigated due to limited material availability). Despite a relatively long scan time, the diffractogram showed no diffraction peaks, the spectrum being dominated by the background due to the glass substrate (we note that F8BT films show clear diffraction peaks under the same experimental conditions with the same apparatus (see Supplementary Information of [33])). This is consistent with XRD results for TFB and other fluorene-triarylamine copolymers, which show no evidence of any crystalline phase [38, 55]. The DSC, optical absorption and XRD results are therefore consistent with PFB and PFMO being amorphous, glassy polymers.

To investigate hole transport in PFB and PFMO in the low-carrier density diode regime, we use the time-of-flight (TOF) technique to measure the nature of transport and its field dependence, and analyze transient SCLC dark injection and TOF results to find the charge-carrier density dependence over the same field range. To investigate hole transport in the high-carrier density diode regime, we use bottom-gate bottom-contact OFETs in both conventional linear and saturation regimes and the low field linear regime, the latter to generate a highly uniform charge carrier density across the length of the channel [5]. To replicate the original studies by Tanase *et al* on P3HT and PPV copolymers [5, 13], OFET samples consisted of standard Si (n^+ doped) / SiO_2 wafer substrates with Au source and drain contacts, with and without contact and channel self-assembled monolayers (SAMs).

One important factor in these types of measurements is to eliminate as far as possible the impact of injection on the measured mobility values. Steady-state SCLC measurements can potentially underestimate the bulk mobility by up to an order of magnitude due to interfacial traps at the polymer / electrode interface [32]. The TOF technique does not involve injection, so avoids this issue. The transient SCLC dark injection technique is based on a transit time like the TOF technique; it is independent of the magnitude of the current signal, which could potentially be reduced by injection efficiency effects [32]. However, we use the SCLC equation to calculate the charge carrier density for the dark injection measurements, and contact resistance effects can also lower the transistor mobility. To avoid this, PFB and PFMO have been selected amongst the fluorene-triarylamine copolymers as they have low ionization potentials of 5.09 and 4.98 eV respectively, minimising the injection barrier with the diode and transistor contacts used in this work [31]. The relatively low mobility of both materials ($\leq 10^{-3}$ cm^2/Vs) also indicates that for the OFETs the channel resistance should dominate over any contact effects. To check any possible injection effects, we also investigated devices with and without an injection barrier lowering thiol SAM attached to the Au source and drain contacts.

We also wish to compare the low- and high- carrier density regimes in diodes (transport vertically through the thin films) and OFETs (transport horizontally at the interface of the thin films). In polycrystalline materials there is no guarantee that the amount of crystallinity, or the crystal size and orientation, will be the same in the bulk film as it is at the interface with a dielectric. Any difference could make charge transport anisotropic, making it difficult to compare results in diodes and OFETs. We note that the amorphous nature of PFB and PFMO avoids this problem, any differences in bulk or interfacial morphology being minimized.

Figure 3a shows typical room temperature hole TOF transients for PFB. Similar results were obtained for PFMO. The TOF transients are non-dispersive and show a clear transit time, in good agreement with previous measurements [31, 39, 41]. Non-dispersive transport indicate that the sheet of photogenerated carriers has reached equilibrium within the transport site DOS distribution as it transits the film [1]. All of the carriers have therefore sampled the deep sites within the DOS. This is in contrast to charge-density dependent transport, in which deep site filling results in many carriers not entering these sites and therefore moving faster. This would also make transport dispersive as the deep sites slowly empty. The shape of the PFB and PFMO TOF transients therefore indicates that transport in the low-density diode regime is not charge-carrier density dependent.

We note that this is supported by transient SCLC dark injection measurements of PFB in the literature. In SCLC measurements the average charge-carrier density in the diode is inversely proportional to the device thickness, and this can be used to test carrier density dependent mobility models [56]. Results for PFB have measured the transient SCLC dark injection mobility over a range of thicknesses from 200 and 1100 nm [39, 40]. Across a wide range of field values, the dark injection mobility for PFB does not change with device thickness. Hence, the mobility in these diodes must be independent of carrier density.

Figure 3b shows typical room temperature OFET transfer and output characteristics for PFB (for PFMO see SI Figure S2). The transistors show well behaved characteristics, with clear linear and saturation regimes.

The TOF mobility was calculated from $\mu_{TOF} = d/(t_{trans}F)$ where t_{trans} is the charge carrier transit time and $F = V/d$ where V is the applied bias and d is the device thickness. The transit time can be taken as the inflexion point time t_t (where the photocurrent starts to decrease from the constant current plateau) (see Figure 3a). However, in previous measurements of PFB, the transit time taken as the quarter-height time $t_{1/4}$ (when the current reaches quarter the plateau value) (see Figure 3a) gave the best agreement with the mobility calculated from transient dark injection measurements for all diode thicknesses between 220 to 1100 nm [39]. To cover all possibilities we have calculated the TOF mobility from both t_t and $t_{1/4}$ (the half-height transit time $t_{1/2}$, when the current reaches half the plateau value, will lie between these values). According to the GDM and correlated GDM the TOF mobility should be field dependent with the form:

$$\mu(F) = \mu_0 \exp A\sqrt{F} \qquad (1)$$

where μ_0 is the zero-field mobility, F is the field and A is a constant [1, 2]. The $\mu_{TOF}(t_0)$ and $\mu_{TOF}(t_{1/4})$ results are shown in Figure 4a and fitted to Equation (1).

To extract the standard values for the FET mobility μ_{FET}, the linear and saturation transfer characteristics were fitted to the standard transistor equations:

$$I_D(lin) = \frac{W\mu_{FET}C_i}{L}(V_G - V_T)V_D \qquad (2a)$$

$$I_D(sat) = \frac{W\mu_{FET}C_i}{2L}(V_G - V_T)^2 \qquad (2b)$$

on a $I_D(lin)$ *vs* V_G and $(I_D(sat))^{1/2}$ *vs* V_G plot (Figure 3c and d), where $I_D(lin)$ and $I_D(sat)$ are the linear and saturation drain currents respectively, V_G is the gate bias, V_T the turn-on voltage, V_D the drain bias, W the channel width, L the channel length, and C_i is the insulator capacitance per unit area. Values are plotted in Figure 4a for field values of $F = V_D/L$, where L is the channel length. Values for OTS treated devices $\mu_{FET}(OTS)$ tend to be higher than those for devices with no channel SAM $\mu_{FET}(No\ SAM)$, although there are exceptions. This is consistent with OTS providing a more controllable dielectric surface with better wetting properties than bare SiO_2 [57]. The variation of $\mu_{FET}(OTS)$ with F for PFB over a range of fields is shown in Figure 4b. The transistor mobility appears to follow Equation (1) and is in good agreement with the variation found for the TOF results. Devices with the contact thiol SAM FTP for PFB and PFMO had mobility values similar to devices with only the bare contacts $\mu_{FET}(No\ SAM)$ (see SI Figure S3). The linear mobility for PFB was also found to remain constant as L was varied from 2.5 to 20 μm, and transmission line method (TLM) analysis to calculate the linear mobility in the absence of contact resistance gave the same value (SI Section S4 and Figures S4a and c). This indicates that if any contact resistance effects are present they are having minimal impact on the extracted mobility for these two low ionization potential polymers at the V_D values used in Figure 4a and b.

The results in Figure 4a and b show two important features. Firstly, for all devices measured, μ_{FET} is approximately equal to or greater than μ_{TOF} at the same field. This is inconsistent with all the charge-carrier density dependent models, which predict that $\mu_{FET} >> \mu_{TOF}$ (the charge carrier density in transistors should be orders of magnitude above that in diodes). Secondly, for the best performing transistors, $\mu_{FET}(F) \approx \mu_{TOF}(F)$. This suggests that in optimised transistors, charge transport at the interface is identical to that in the bulk. This is a characteristic of a charge-carrier density independent mobility.

We then measured the variation of μ with charge carrier density p in both diodes and transistors, and explored these results within the Vissenberg and Matters framework using the model developed by Tanase *et al* [5].

For the diodes, transient dark injection SCLC and TOF mobility values μ_{DI} and μ_{TOF} for device thicknesses between 200 and 1750 nm and three different field values (100, 200 and 300 kV/cm) were taken from previous literature measurements [39-41]. The average dark injection hole density p_{DI} was calculated according to SCLC theory using the equation:

$$p_{DI} = \frac{3}{2}\frac{\varepsilon_r \varepsilon_0}{e}\frac{F}{d} \qquad (3)$$

where ε_r and ε_0 are the relative dielectric and vacuum permittivity respectively and e is the charge on the electron (we take ε_r = 3.5). The TOF carrier density was calculated from the total charge in the measured transient and assuming a photogenerated charge sheet thickness equal to the absorption depth (≈ 100 nm). (The results of this analysis for PFB at three different field values are shown in SI Figure S5. As discussed above, these clearly indicate a charge carrier density independent mobility in the low carrier density diode regime.)

For the transistors, it is important to measure the mobility in the low drain bias regime to achieve a uniform charge density along the length of the channel. The linear-regime transfer characteristics for PFB and PFMO transistors were measured at drain bias V_D values of -0.5 and -2 V. The linear-regime FET mobility was calculated as previously described [5]. The FET charge-carrier density per unit volume was calculated from:

$$p_{FET} = \frac{-C_i\left(V_G - V_0 - V_D/2\right)}{e\Delta x} \qquad (4)$$

where V_0 is the gate voltage where the device turns on (ie. the drain current exceeds the off current), and Δx is the channel depth (which we take as 2 nm from work by the authors of the approach [5, 13]). Data is only plotted for V_G-$V_0 \geq 2V_D$ to maintain a uniform charge density in the channel. p_{FET} values varied from $5\text{x}10^{17}$ to $3\text{x}10^{19}$ cm^{-3}, covering the range previously studied [5,13]. Note that for V_D = -0.5 V, data could only be recorded for the higher mobility transistors. It also became very noisy above p_{FET} values of $3\text{x}10^{18}$ cm^{-3}, so has not been plotted above this point. Additionally, the lower limit of $5\text{x}10^{17}$ cm^{-3} is set by the inaccuracy in estimating V_0 of about ±0.5 V. In PFB V_D = -0.5 V also gave a slightly lower mobility value than V_D = -2 V, most likely due to injection effects at the low field. This was not an issue for PFMO, which has a smaller ionization potential than PFB.

Dark injection, TOF and representative transistor mobility results are plotted against charge density in Figures 5a and b for PFB and PFMO respectively. The horizontal dashed line is the zero-field mobility $\mu_0(t_{1/4})$.

To fit our results to the Tanase *et al* model we require the Gaussian transport DOS width σ_{DOS} for PFB and PFMO. This has been measured within our group using the variation of the TOF mobility with field and temperature [39, 58]. Analysis using the Bässler Gaussian disorder model (GDM) gives values for the PFB and PFMO DOS width of 0.085 and 0.11 eV respectively [1, 39, 58]. Converting to the correlated GDM (a factor of 10/9) gives values of σ_{DOS} of 0.094 and 0.12 eV respectively [1, 2]. To find the Vissenberg and Matters exponential DOS distribution characteristic temperature T_0 we use the comparative method used by Tanase *et al.*. We take a Gaussian DOS distribution with a total integrated site density of N = 3 x 10^{20} cm^{-3} and width σ_{DOS} from the correlated GDM [5]. We integrate across the distribution and the Fermi-Dirac function at room temperature to find the position of the Fermi level at the minimum and maximum values of p_{FET}. We then fit the Gaussian DOS between these two values to an exponential DOS of form $N_{exp}exp(-E/k_BT_0)$ where E is energy, N_{exp} density and k_B Boltzmanns constant. This results in values of T_0 of 460 and 610 K for PFB and PFMO respectively. $\mu_{TOF}(t_{1/4})$ gives the best agreement with the bulk SCLC dark injection mobility [39]. Therefore, by extrapolation from $\mu_0(t_{1/4})$ at 10^{16} cm^{-3}, we use these values of T_0 to calculate the values of the FET mobility $\mu_{FET}(model)$ predicted by the model using:

$$\mu_{FET}(model) = \mu_0 \left(\frac{p_{FET}}{p_0} \right)^m$$
$$m = \frac{T_0}{T} - 1 \qquad (5)$$

where μ_0 and p_0 are constants and T is temperature. This is shown in Figure 5a and b.

The results in Figure 5 show four important features.

Firstly, all the measured FET mobility values for PFB and PFMO lie 100 – 1000 times below $\mu_{FET}(model)$. Secondly, the measured FET mobility values do not obey the predicted power-law relationship from the model. Indeed, they do not obey any power-law, the FET mobility being approximately constant with increasing density on the log-log scale in Figure 5a and b. The same result was found for all PFB and PFMO transistors measured, both with and without OTS or FTP. Thirdly, the values of μ_{FET} (recorded at low fields) correspond well with $\mu_0(t_{1/4})$. PFMO is in excellent agreement, while PFB at $F = 2$ kVcm^{-1} is within a factor of 2. This is consistent with the results already discussed in Figure 4. Fourthly, the DI and TOF mobility values at a given field for PFB do not vary with charge-carrier density; the smaller data set for PFMO is consistent with this. This reflects the early discussion of the dark injection literature results.

Overall, the results in Figure 4 and 5 are consistent with a weakly field dependent, charge-carrier density independent mobility, in which transport at the dielectric interface in optimised transistors is the same as that in the bulk.

We do note that in the Tanase *et al* model the effect of dipolar disorder DOS broadening at the semiconductor-dielectric interface proposed by Veres *et al* [59] is not included. In this model static dipolar disorder in the dielectric increases the DOS width of the semiconductor in the FET channel. This would mean that $\sigma_{DOS}(FET) > \sigma_{DOS}$, increasing T_0 and the slope of $\mu_{FET}(model)$. Considering Figure 5a and b, the inclusion of dipolar disorder DOS broadening would therefore make the model deviate even more from the experimentally measured μ_{FET} values.

Another key prediction of the charge-carrier density dependent mobility models is that the activation temperature for charge transport should decrease with increasing carrier density [9]. One would expect the three orders of magnitude difference in carrier density to make the activation energy in the high-density transistor regime ($\approx 10^{19}$ cm^{-3}) approximately half that in the low-density diode regime ($\approx 10^{16}$ cm^{-3}) [9]. Temperature measurements were therefore conducted on PFB diodes and transistors in the range from 298 to 403K (see SI Figure S6). The zero-field TOF mobility was found to have an activation energy of 0.20 eV (GDM σ_{DOS} equivalent of 0.08 eV), the zero-field steady-state SCLC mobility giving similar values. The linear and saturation FET mobility were found to have an activation energy of 0.21 and 0.22 eV respectively (GDM σ_{DOS} equivalents of 0.089 and 0.087 eV respectively). This is not consistent with a charge carrier density mobility. It is instead more consistent with a charge carrier density independent mobility in which the energy landscape seen by the carriers does not change with density. Intriguingly similar measurements of the well known vacuum sublimed glassy diamine small molecule N,N'-diphenyl-N,N'-bis(3-methylphenyl)1-1'-biphenyl-4,4'-diamine (TPD) show exactly the same result [60].

We also applied Equation (5) to the standard gradual channel approximation used to calculate transistor characteristics. For a constant mobility μ_{FET} this results in Equations (2a) and (2b). For a charge carrier density dependent mobility given by Equation (5) this results instead in the approximate forms:

$$I_D(lin) \approx \frac{W\mu_0 C_i}{L} \left(\frac{C_i}{e\Delta x p_0} \right)^m \left(V_G - V_T \right)^{m+1} V_D \qquad (6a)$$

$$I_D(sat) = \frac{W\mu_0 C_i}{(m+2)L} \left(\frac{C_i}{e\Delta x p_0} \right)^m \left(V_G - V_T \right)^{m+2} \qquad (6b)$$

(see SI derivation S7). On a standard $I_D(lin)$ *vs* V_G and $(I_D(sat))^{1/2}$ *vs* V_G plot, Equations (6a) and (6b) should lead to non-linear characteristics where both $I_D(lin)$ and $(I_D(sat))^{1/2}$ follow a power law with V_G. This can be taken as a marker of a charge carrier density dependent mobility in any FET results. For a charge carrier density independent mobility, $m = 0$ and Equations (6a) and (6b) reduce to (2a) and (2b).

(However, we do note that the mobility-edge model, based on the relationship between free carriers in transport states and trapped carriers in an exponential distribution of deep states of characteristic temperature T_0,

produces exactly the same power-law relationships between $I_D(lin)$ and V_G and $I_D(sat)$ and V_G in Equations (6a) and (6b), with only the prefactors varying (see SI derivation S8). This type of power-law relationship for discrete transport states with an exponential trap distribution has been noted previously and applied to pentacene OFETs by Horowitz *et al* [61]).

P3HT was one of the polymers originally fitted to Equation (4) by Tanase *et al* [5]. We measured the transfer characteristics of a reference sample of P3HT, and explored the applicability of Equations (6a) and (6b) (see SI Figure S9). For this polycrystalline polymer, the $I_D(lin)$ and $(I_D(sat))^{1/2}$ *vs* V_G characteristics are clearly non-linear, and Equations (6a) and (6b) gave a good fit for $T_0 = 540$ K.

PFB and PFMO instead have highly linear $I_D(lin)$ and $(I_D(sat))^{1/2}$ *vs* V_G characteristics (Figure 3c and d) and follow Equations (2a) and (2b). This is consistent with poly(triarylamine) and other fluorene-triarylamine copolymers, which also all have highly linear characteristics [38]. Hence, the transfer characteristics alone indicate that the mobility of these polymers does not follow Equation (5).

If PFB and PFMO have a charge carrier-density independent mobility, the question arises as to how this can occur for a disordered amorphous material with a Gaussian DOS width of order 0.1 eV. A charge carrier-density dependent mobility works on the physical principal that as the carrier density increases, the probability of a deep site in the DOS sites being occupied by a carrier increases. Other carriers in the DOS are therefore less likely to visit those sites, and be slowed down by having to escape from them. The average mobility of the whole carrier ensemble therefore increases as their number increases. For a charge carrier-density independent mobility this cannot occur. The range of energies of the DOS sites visited by the carriers cannot vary as the number of carriers increases. The effective energy landscape needs to be much smoother.

One possibility is to include the effect of polarons. If the polaron activation energy is significant compared to the DOS width it would smooth out the energy landscape. It would also offer an elegant solution in explaining how density dependent and independent mobility materials can occur via the reorganization energy. TOF results for PFB and similar fluorene-triarylamine copolymers have been successfully fitted to the polaronic correlated GDM in the low-density regime, giving a polaron activation energy greater than the DOS width [43]. For this situation, the multi-carrier effective-medium approximation (EMA) analytical theory does indeed predict a charge-carrier density independent mobility, exactly as we observe [6]. However, it also predicts a field-independent mobility, which we do not observe [12]. A percolation model for transport in an uncorrelated Gaussian DOS also predicts a charge carrier-density dependant mobility even with a polaronic contribution, suggesting this cannot explain the results in this work [8].

Another possibility is correlated disorder. With correlated disorder the nearest-neighbour transport site energies are correlated with each other, smoothing out the energy landscape as shown in Figure 1a. In an amorphous polymer this could be envisaged to occur by similarities in the nearest-neighbour chain conformation resulting in similarities in the conjugation length. This could again vary between different materials depending on backbone stiffness and interchain and sidegroup packing. TOF results for PFB and similar fluorene-triarylamine copolymers have been successfully fitted to the correlated GDM in the low-density regime [43]. Steady-state SCLC diode measurements of fluorene-triarylamine copolymers have also been successfully fitted to the correlated and uncorrelated EGDM [44]. The EGDM with correlated disorder (ECDM) does predict a mobility which is field dependent and charge-carrier independent (we note that analysis of the experimentally measured transport parameters for PFB and PFMO within the ECDM framework (see SI Section S10) does, assuming an interchain hopping distance of 1 nm and a hopping attempt frequency of 10^{14} s^{-1}, yield not unreasonable values for the wavefunction decay length of 0.14 to 0.29 nm, respectively). The EMA theory with correlated disorder also predicts a mobility which is field dependent and effectively charge-carrier independent at the DOS widths found for PFB and PFMO [11]. Hence, the presence of correlated disorder might offer a possible explanation of charge-carrier density independent transport in amorphous fluorene-triarylamine copolymers. Recent structural investigations of a non-crystalline high mobility polymer show long-range alignment between the chains [62]. Such structural correlations may therefore be key to explaining charge transport in amorphous conjugated polymers.

Summary

We have investigated the charge carrier-density dependency of hole transport in two amorphous fluorene-triarylamine copolymer glasses. This is in both the low-density diode regime (10^{14} to 10^{17} cm^{-3}) using time-of-flight (TOF) measurements and analysis of transient dark injection (DI) literature results, and in the high-density transistor regime (10^{17} to 10^{20} cm^{-3}) using OFET measurements. We have also explored these results within the Vissenberg and Matters framework using the model developed by Tanase *et al* [5]. This relates

the magnitude and Gaussian DOS width for transport in the diode regime to the magnitude and exponential DOS density-mobility power-law for transport in the transistor regime.

Firstly, we observe that: (i) the TOF transients of PFB and PFMO are non-dispersive; (ii) the DI mobility for PFB does not vary with carrier density (the smaller data set for PFMO is consistent with this). Both results are consistent with a density independent mobility in the low-density diode regime. Secondly, we observe that for PFB and PFMO the FET mobility remains approximately constant with carrier density. This is consistent with a density independent mobility in the high-density transistor regime. Thirdly, we observe that: (i) for PFB and PFMO the FET mobility for the best transistors is equal to the TOF mobility at the same field; (ii) for PFB the FET and TOF mobility have the same temperature dependency. Both results are consistent with a density independent mobility across both regimes. Fourthly, we observe that for PFB and PFMO: (i) the FET mobility does not follow the density-mobility power-law predicted by the model; (ii) the magnitude of the FET mobility is two to three orders of magnitude below that predicted by the model. Both results are again consistent with a density independent mobility across both regimes.

Our results for these two amorphous fluorene-triarylamine copolymers are therefore consistent with a weakly field dependent, charge-carrier density independent mobility. This is unlike results for many other conjugated polymers, which appear to have a field dependent, charge-carrier density dependent mobility. We note that this density dependent mobility may also be a property linked to the polycrystalline morphology of many of these materials.

This charge-carrier density independent mobility could potentially be explained by correlated disorder in the fluorene-triarylamine copolymers. If molecular packing and backbone rigidity favour a more slowly varying chain morphology, nearest-neighbour conjugation lengths will be correlated, resulting in a smoothly varying transport state energy landscape. This suggests that long-range order is an important factor in determining charge transport in amorphous conjugated polymers.

Experimental

Time-of-Flight measurements. Samples were prepared by spin-coating PFB and PFMO at 1500 rpm from *p*-xylene solutions at concentrations of 60 to 120 mg/ml. This was followed by a solvent removal baking step (100°C, 10 minutes). TOF samples consisted of ITO on glass substrates (purchased from CRL Optics; cleaned as described below for Si wafer substrates), spincoated polymer films (thickness *d* of 1 to 2 μm as measured by a Dektak surface profiler) and thermally evaporated semitransparent (40 nm thick) Al top metal contacts. TOF measurements at room temperature and with temperature were conducted as described previously using a Quantel ND:YAG ns-pulsed laser (excitation wavelength 355 nm), an in-house fabricated DC source and a Tektronics TDS 3052 oscilloscope, and a helium exchange-gas Oxford Instruments Opstitat cryostat [39, 43].

Transistor measurements. Samples were prepared by spin-coating PFB and PFMO at 3000 rpm from *p*-xylene, *o*-xylene or chloroform solutions at concentrations of 5 or 10 mg/ml. This was followed by a solvent removal baking step (100°C, 10 minutes). Film thicknesses were 40 to 60 nm (as measured by a Dektak surface profiler). FET samples consisted of standard Si (n^+ doped) / SiO_2 wafer substrates with Au source and drain contacts (purchased from the Fraunhofer IPMS, Germany). Channel lengths *L* were 2.5, 5, 10 or 20 μm, channel widths *W* were 0.2, 1 or 2 cm, and SiO_2 thickness was 210 or 230 nm. The surface was cleaned prior to polymer deposition using a series of solvent washing and drying steps (water, acetone, IPA; dried with pressurized N_2) followed by ozone plasma treatment for 10 minutes. For some devices, an octyltrichlorosilane (OTS) self-assembled monolayer (SAM) was deposited on the SiO_2 surface (substrates immersed for 15 minutes at 60°C in 10mM solution in toluene or hexadecane; then sequentially rinsed in toluene, acetone and IPA to remove excess material). For other devices, a 4-fluorothiophenol (FTP) SAM was deposited on the surface of the Au contacts (substrates immersed for 14 hours in 1mM solution in ethanol; then rinsed thoroughly in ethanol and cleaned in an ultrasonic bath to remove excess material). Contact angle measurements were used to confirm the presence and quality of the SAM layers using a Kruss drop shape analysis system. FET characteristics at room temperature and with temperature were recorded as described previously in a nitrogen atmosphere (PFB and PFMO OTS, No SAM, FTP devices) or in ambient (PFB OTS devices were found to be ambient stable) using an Agilent 4155C or 4156C semiconductor parameter analyser, and a hot-stage mounted in a nitrogen filled glove box [57, 63].

Materials. PFB and PFMO samples were supplied by the Sumitomo Chemical Co.. The P3HT sample was supplied by Merck. All solvents and SAMs were purchased from Aldrich.

Materials characterisation. DSC measurements were carried out using a Mettler Toledo DSC1H at heating and cooling rates of 10°C/min using 2.12 and 2.23 mg of PFB and PFMO, respectively. Optical absorbance spectra

were recorded using a Bentham single-beam UV–vis system. For the solution spectra, solutions were prepared at a concentration of 0.1 mg/ml in toluene. For thin film spectra, films were made by drop-casting from 1mg/ml in toluene onto clean glass slides. XRD measurements used a Panalytical X'Pert Pro diffractometer operating at 40 kV and 40 mA with Ni filtered CuKα radiation. The PFB was cast from 38 mg/ml in toluene solution via spin coating and then annealed for 1 hour at 150°C (above the glass transition at 132°C). Film thickness was measured to be 330 nm.

Acknowledgements

The authors would like to thank the Sumitomo Chemical Co for supplying PFB and PFMO samples and Merck for supplying the P3HT sample. We also thank the UK Engineering and Physical Sciences Research Council (UK EPSRC) for funding Ruth Rawcliffe (award number GR/P00772/01), Alexander Guite (award number EP/P502500/1) and Abhimanyu Mukherjee (award number EP/M506345/1) through Doctoral Training Award studentships and Jorge C. D. Faria (award number EP/G037515/1) through a Plastic Electronics Doctoral Training Centre studentship.

References

[1] H. Bässler, *Phys. Stat. Sol. (b)* **1993**, *175*, 15
[2] S. V. Novikov, D. H. Dunlap, V. M. Kenkre, P. E. Parris, A. V. Vannikov, *Phys. Rev. Lett.* **1998**, *81*, 4472
[3] P. E. Parris, V. M. Kenkre, D. H. Dunlap, *Phys. Rev. Lett.* **2001**, *87*, 126601
[4] M. C. J. M. Vissenberg, M. Matters, *Phys. Rev. B* **1998**, *57*, 12964
[5] C. Tanase, E. J. Meijer, P. W. M. Blom, D. M. de Leeuw, *Phys. Rev. Lett.* **2003**, *91*, 216601
[6] I. I. Fishchuk, V. I. Arkhipov, A. Kadashchuk, P. Heremans, H. Bässler, *Phys. Rev. B* **2007**, 76, 045210
[7] W. F. Pasveer, J. Cottaar, C. Tanase, R. Coehoorn, P. A. Bobbert, P. W. M. Blom, D. M. de Leeuw, M. A.J. Michels, *Phys. Rev. Lett.* **2005**, *94*, 206601
[8] J. Cottaar, L. J. A. Koster, R. Coehoorn, P. A. Bobbert, *Phys. Rev. Lett.* **2011**, *107*, 136601
[9] I. I. Fishchuk, A. Kadashchuk, J. Genoe, M. Ullah, H. Sitter, Th. B. Singh, N. S. Sariciftci, H. Bässler, *Phys. Rev. B* **2010**, *81*, 045202
[10] M. Bouhassoune, S. L. M. van Mensfoort, P. A. Bobbert, R. Coehoorn, *Org. Elec.* **2009**, *10*, 437
[11] I. I. Fishchuk, A. Kadashchuk, M. Ullah, H.Sitter, A. Pivrikas, J. Genoe, H. Bässler, *Phys. Rev. B* **2012**, *86*, 045207
[12] I. I. Fishchuk, A. Kadashchuk, V. N. Poroshin, H. Bässler, *Phil. Mag.* **2010**, *90*, 1229
[13] C. Tanase, P. W. M. Blom, D. M. de Leeuw, E. J. Meijer, *Phys. Stat. Sol. (a)* **2004**, *201*, 1237
[14] I. Katsouras, A. Najafi, K. Asadi, A. J. Kronemeijer, A. J. Oostra, L. J. A. Koster, D. M. de Leeuw, P. W. M. Blom, *Org. Elec.* **2013**, *14*, 1591
[15] T. Leitjens, J. Lim, J. Teuscher, T. Park, H. J. Snaith, *Adv. Mater.* **2013**, *25*, 3227
[16] H. Sirringhaus, P. J. Brown, R. H. Friend, M. M. Nielsen, K. Bechgaard, B. M. W. Langeveld-Voss, A. J. H. Spiering, R. A. J. Janssen, E. W. Meijer, P. Herwig, D. M. deLeeuw, *Nature,* **1999**, *401*, 685
[17] A. R. Aiyar, J.-I. Hong, R. Nambiar, D. M. Collard, E. Reichmanis, *Adv. Funct. Mater.* **2011**, *21*, 2652–2659
[18] E. J. W. Crossland, K. Tremel, F. Fischer, K. Rahimi, G. Reiter, U. Steiner, S. Ludwigs, *Adv. Mater.* **2012**, *24*, 839–844
[19] H. Yang, E. Glynos, B. Huang, P. F. Green, *J. Phys. Chem.* **2013**, *117*, 9590
[20] C. Y. Yang, F. Hide, M. A. Diaz-Garcia, A. J. Heeger, Y. Cao, *Polymer* **1998**, 39, 2299
[21] A. R. Inigo, C. C. Chang, W. Fann, J. D. White, Y. S. Huang, U. S Jeng, H. S. Sheu, K. Y. Peng, S. A. Chen, *Adv. Mater.* **2005**, *17*, 1835
[22] Y. F. Huang, *et al Adv. Funct. Mater.* **2007**, *17*, 2902
[23] U. Jeng, C.-H. Hsu, H.-S. Sheu, H.-Y. Lee, A. R. Inigo, H. C. Chiu, W. S. Fann, S. H. Chen, A. C. Su, T.-L. Lin, K. Y. Peng, S. A. Chen, *Macromolecules* **2005**, *38*, 6566
[24] M. Morana, M. Wegscheider, A. Bonanni, N. Kopidakis, S. Shaheen, M. Scharber, Z. Zhu, D. Waller, R. Gaudiana, C. Brabec, *Adv. Funct. Mater.* **2008**, *18*, 1757
[25] C. Elschner, A. A. Levin, L.Wilde, J. Grenzer, C. Schroer, K. Leoa, M. Riede, *J. Appl. Cryst.* **2011**, *44*, 983–990
[26] R. Matsubara, M. Sakai, K. Kudo, N. Yoshimoto, I. Hirosawa, M. Nakamura, *Organic Electron.*, **2011**, *12*, 195
[27] R. Noriega1, J. Rivnay, K. Vandewal, F. P. V. Koch, N. Stingelin, P. Smith, M. F. Toney, A. Salleo, *Nat.*

Mater. **2013**, *12*, 1038
[28] S. Yogev, R. Matsubara, M. Nakamura, Y. Rosenwaks, *Organic Electron.* **2010**, *11*, 1729
[29] A. Salleo, T. W. Chen, A. R. Völkel, Y. Wu, P. Liu, B. S. Ong, R. A. Street, *Phys. Rev. B* **2004**, *70*, 115311
[30] R. A. Street, J. E. Northrup, A. Salleo, *Phys. Rev. B* **2005**, *71*, 165202
[31] M. Redecker, D. D. C. Bradley, M. Inbasekaran, W.W. Wu, E. P. Woo, *Adv. Mater.* **1999**, *11*, 241
[32] M. J. Harding *et al.*, *Adv. Funct. Mater.* **2010**, *20*, 119
[33] J. C. D. Faria, A. J. Campbell, M. A. McLachlan, *J. Mater. Chem. C* **2015**, *3*, 4945
[34] J. C. D. Faria, A. J. Campbell, M. A. McLachlan, *Adv. Funct. Mater.* **2015**, *25*, 4657
[35] A. C. Morteani, A. S. Dhoot, J.-S. Kim, C. Silva, N. C. Greenham, C. Murphy, E. Moons, S. Cina, J. H. Burroughes, R. H. Friend, *Adv. Mater.* **2003**, *15*, 1708
[36] J.-S. Kim, L. Lu, P. Sreearunothai, A. Seeley, K.-H. Yim, A. Petrozza, C. E. Murphy, D. Beljonne, J. Cornil, R. H. Friend, *J. Am. Chem. Soc.* **2008**, *130*, 13120
[37] J.-S. Kim, R. H. Friend, I. Grizzi J. H. Burroughes, *Appl. Phys. Lett.* **2005**, *87*, 023506
[38] W. Zhang, J. Smith, R. Hamilton, M. Heeney, J. Kirkpatrick, K. Song, S. E. Watkins, T. Anthopoulos, I. McCulloch, *J. Am. Chem. Soc.* **2009**, *131*, 10814
[39] D. Poplavskyy, J. Nelson and D. D. C. Bradley, *Macromol. Symp.* **2004**, *212*, 415
[40] A. Papadimitratos, H. H. Fong, G. G. Malliaris, A. Yakimov, A. Duggal, *Appl. Phys. Lett.* **2007**, *91*, 042116
[41] A. J. Campbell, D. D. C. Bradley, H. Antoniadis, M. Inbasekaran, W.W. Wu, E. P. Woo, *Appl. Phys. Lett.* **2000**, *76*, 1734
[42] S. Logan, J. E. Donaghey, W. Zhang, I. McCulloch, A. J. Campbell *J. Mater. Chem. C* **2015**, *3*, 7526
[43] R. U. A. Khan, D. Poplavskyy, T. Kreouzis, D. D. C. Bradley, *Phys. Rev. B* **2007**, *75*, 035215
[44] R. J. de Vries, S. L. M. van Mensfoort, V. Shabro, S. I. E. Vulto, R. A. J. Janssen, R. Coehoorn, *Appl. Phys. Lett.* **2009**, *94*, 163307
[45] M . Bernius, M. Inbasekaran, E. Woo, W. Wu, L. Wujkowski, *J. of Mater. Sci.: Materials in Electronics,* **2000**, *11*, 111
[46] Y. Zhao, G. Yuan, P. Roche, M. Leclerc *Polymer* **1995**, *36*, 2211
[47] S. H. Chen, A. C. Su, C. H. Su, S. A. Chen, *Macromol.* **2005**, *38*, 379
[48] C. L. Donley, J. Zaumseil, J. W. Andreasen, M. M. Nielsen, H. Sirringhaus, R. H. Friend, J.-S. Kim, *J. Am. Chem. Soc.* **2005**, *127*, 12890
[49] G. C. Faria, E. R. de Azevedo, H. von Seggern, *Macromol.* **2013**, *46*, 7865
[50] O. Werzer, H.-G. Flesch, D.-M. Smilgies, R. Resel, *J. of Polymer Sci.: Part B: Polymer Physics* **2009**, *47*, 1599
[51] L. Kindera, J. Kanickia, P. Petroff, *Synth. Met.* **2004**, *146*, 181
[52] F. C. Spano, *Chem. Phys.* **2006**, *325*, 22
[53] J. Clark, J.-F. Chang, F. C. Spano, R. H. Friend, C. Silva, *Appl. Phys. Lett.* **2009**, *94*, 163306
[54] M. Grell, D.D.C. Bradley, X. Long, T. Chamberlain, M. Inbasekaran, E.P. Woo, M. Soliman*, Acta Polym.* **1998**, *49*, 439
[55] D. Liu, R. O. Orozco, T. Wang, *Phys. Rev. E* **2013**, *88*, 022601
[56] P. W. M. Blom, C. Tanase, D. M. de Leeuw, R. Coehoorn, *Appl. Phys. Lett.* **2005**, *86*, 092105
[57] R. Rawcliffe, M. Shkunov, M. Heeney, S. Tierney, I. McCulloch, A. J. Campbell, *Chem. Comm.* **2008**, *7*, 871
[58] Robert Peter Stanley, PhD Thesis, Imperial College London 2012
[59] J. Veres, S. D. Ogier, S. W. Leeming, D. C. Cupertino, S. M. Khaffaf, *Adv. Funct. Mater.* **2003**, *13*, 199
[60] C. H. Cheung, K. K. Tsung, K.C. Kwok, S. K. So, *Appl. Phys. Lett.* **2008**, *93*, 083307
[61] G. Horowitz, P. Lang, M. Mottaghi, H. Aubin, *Adv. Funct. Mater.* **2004**, *14*, 1069
[62] Zhang et al, *Nat. Comm.* **2013**, *4*, 2238
[63] X. Wang, K. Wasapinyokul, W. D. Tan, R. Rawcliffe, A. J. Campbell, D. D. C. Bradley, *J. Appl. Phys.* **2010**, *107*, 024509
[64] D. Natali and M. Caironi, *Adv. Funct. Mater.* **2012**, *24*, 1357
[65] R. Coehoorn and P. A. Bobbert, *Phys. Status Solidi A* **2012**, *209*, 2354
[66] M. Mladenović and N. Vukmirović, *Adv. Funct. Mater.* **2015**, *25*, 1915

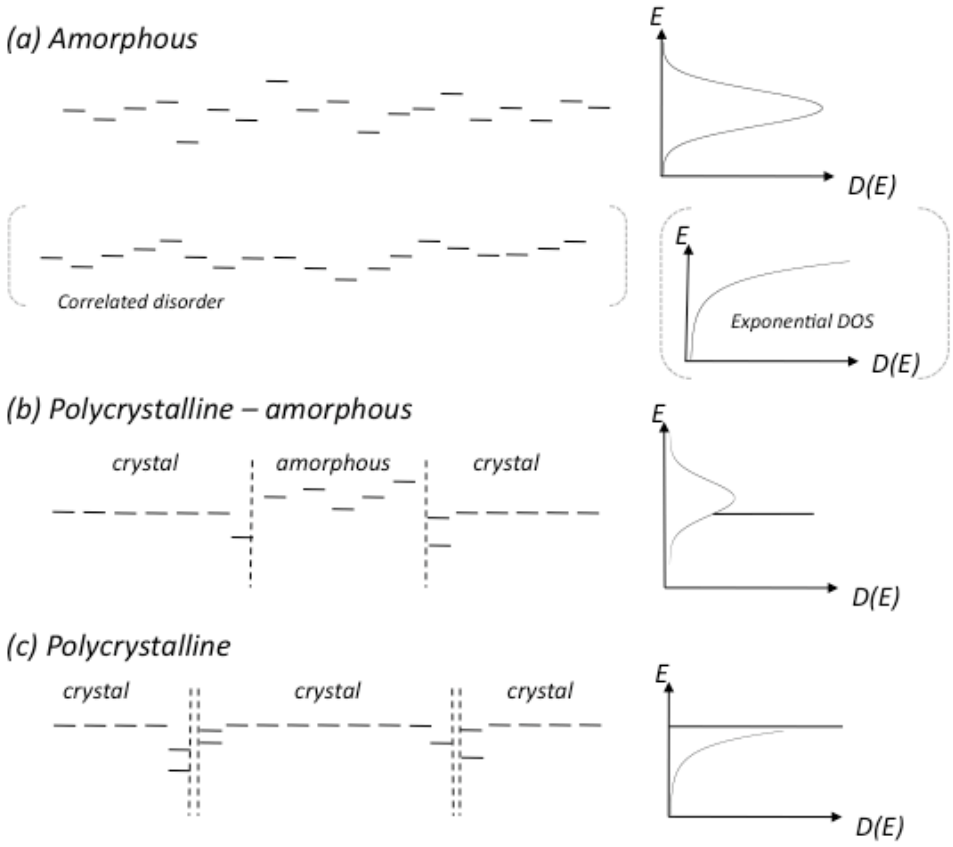

Figure 1. Representations of the transport state energy landscape and density of states (DOS) distribution *D(E)* for different disordered organic semiconductors. (a) A pure amorphous, glassy material with uncorrelated disorder and a Gaussian DOS. Also shown is the correlated disorder variant, where the energy of nearest-neighbour states forming a Gaussian DOS are not random (uncorrelated) but correlated. An exponential DOS is also sometimes used as an approximation to a Gaussian DOS. (b) A mixed polycrystalline-amorphous system consisting of small crystallites or aggregates embedded in a varying fraction of amorphous material. (c) A polycrystalline material consisting of only small crystallites.

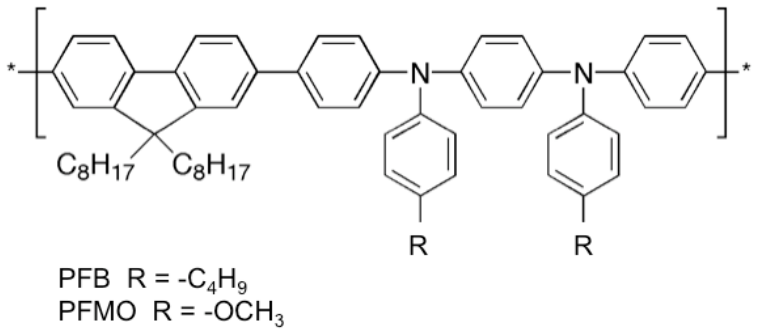

PFB R = $-C_4H_9$
PFMO R = $-OCH_3$

a)

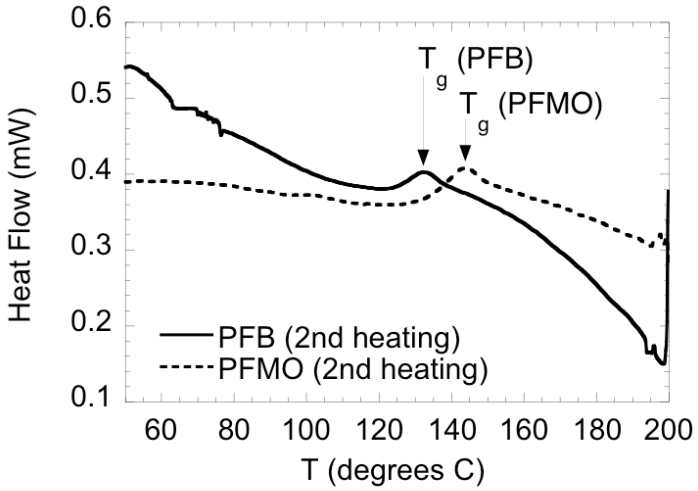

b)

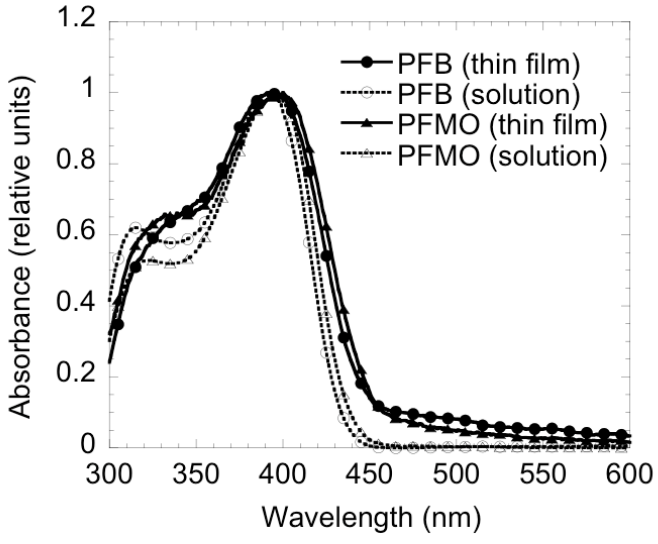

c)

Figure 2. a) Chemical structure of PFB and PFMO. b) Differential scanning calorimetry (DSC) spectra of PFB and PFMO. This is for the 2nd heating run. c) Optical absorption spectra of PFB and PFMO solutions in toluene and thin-films.

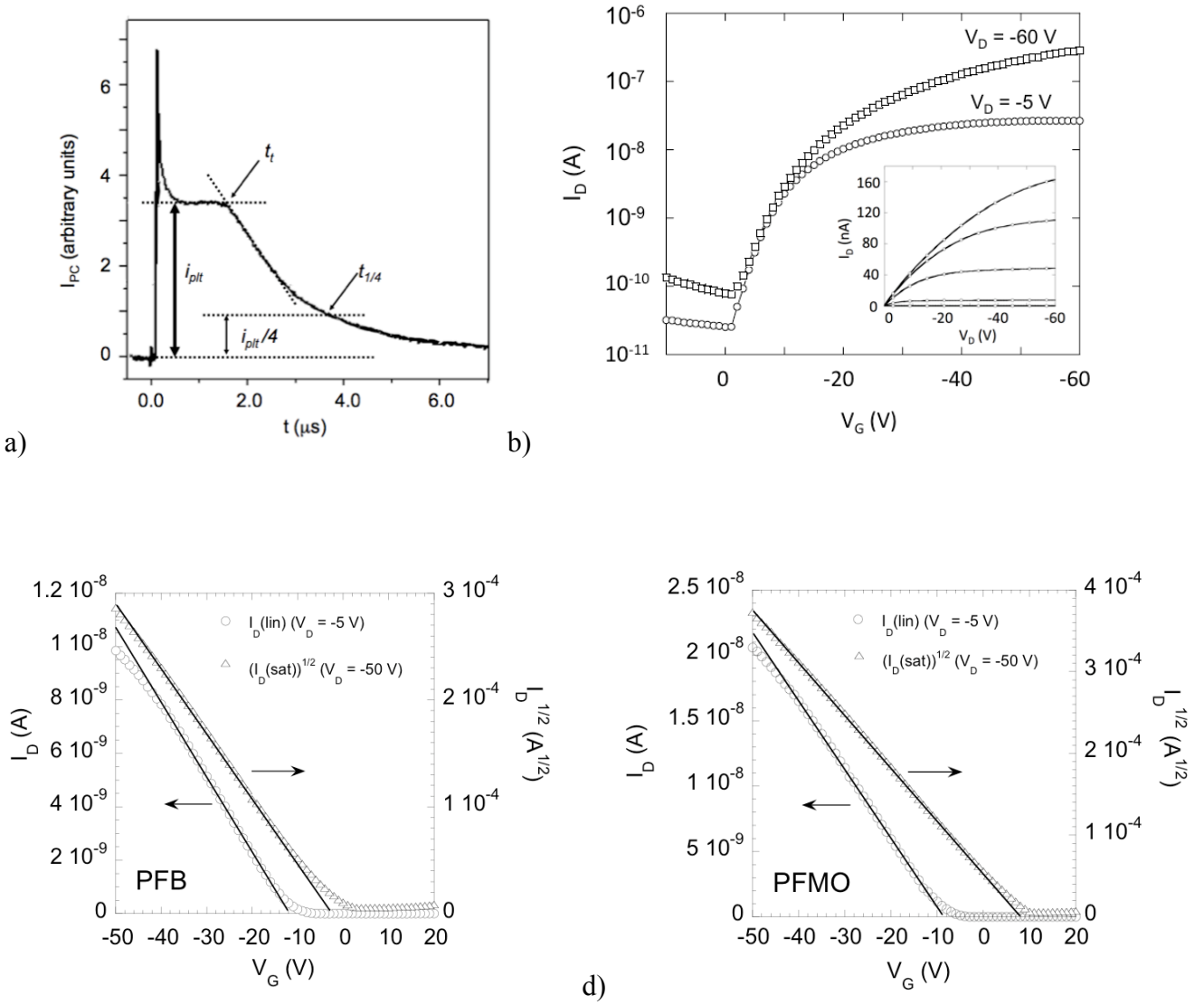

Figure 3. a) Representative time-of-flight (TOF) transient for hole transport in PFB. b) Representative transfer characteristics for a PFB field-effect transistor. Inset shows output characteristics (between V_G = 0 and -60 V at -15 V intervals). c), d) Variation of the linear regime drain current I_D(lin) and the square-root of the saturation regime drain current $(I_D(sat))^{1/2}$ with gate voltage V_G for c) PFB and d) PFMO. Lines are fits to Equations (2a) and (2b).

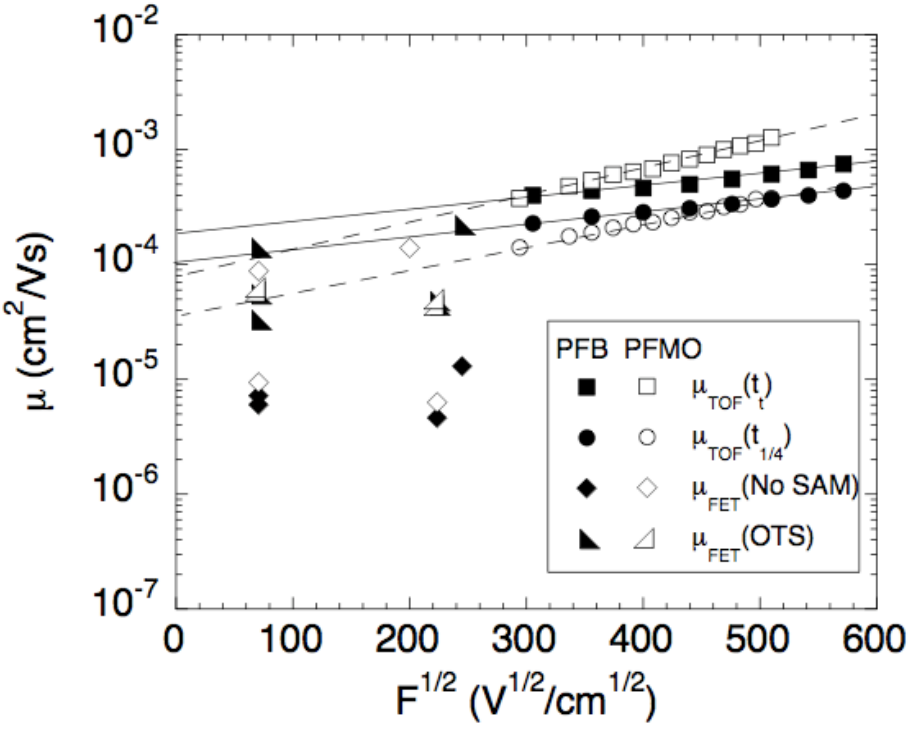

a)

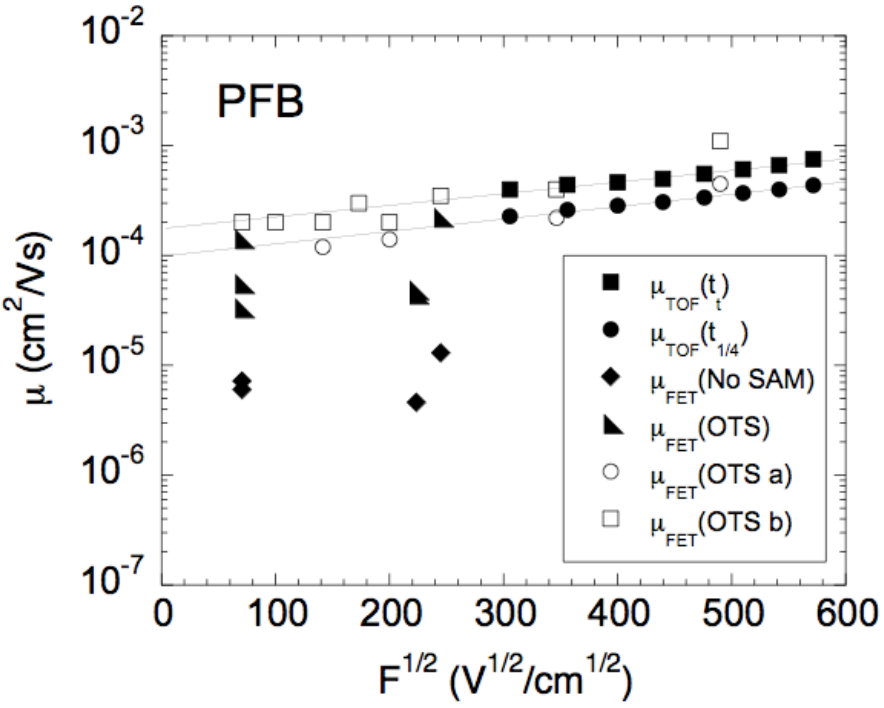

b)

Figure 4. a) Variation of PFB and PFMO time-of-flight (TOF) and linear and saturation field-effect transistor (FET) mobility μ with the square-root of the applied field F. Solid and dashed lines are fits of Equation (1) to the TOF results. b) As 4a) for PFB but including additional data for transistors with a range of different channel lengths (L = 2.5, 5, 10 and 20 μm). OTS a and OTS b are from two different device fabrication runs.

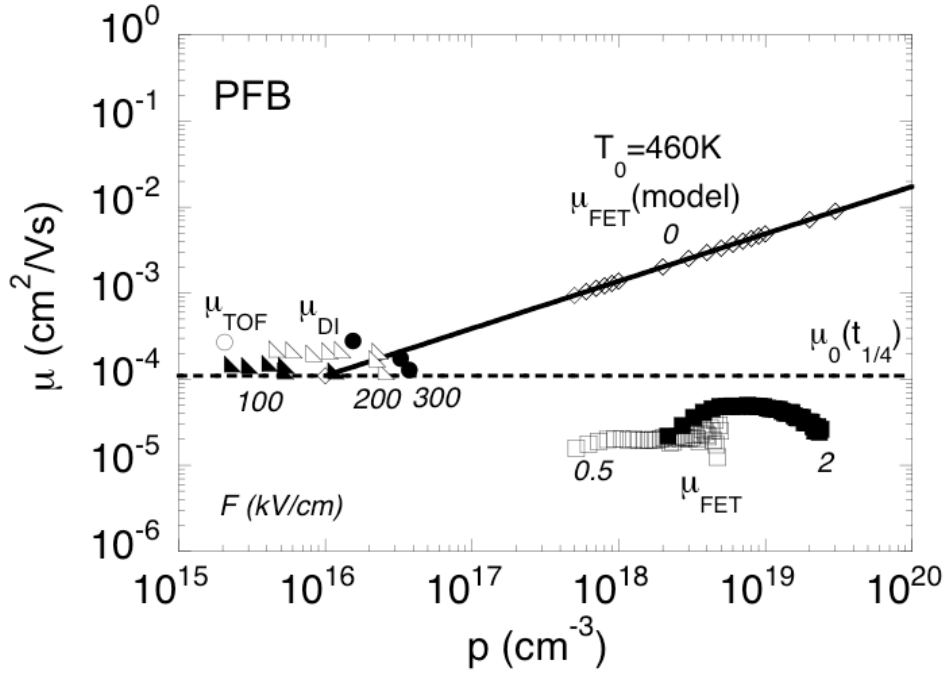

a)

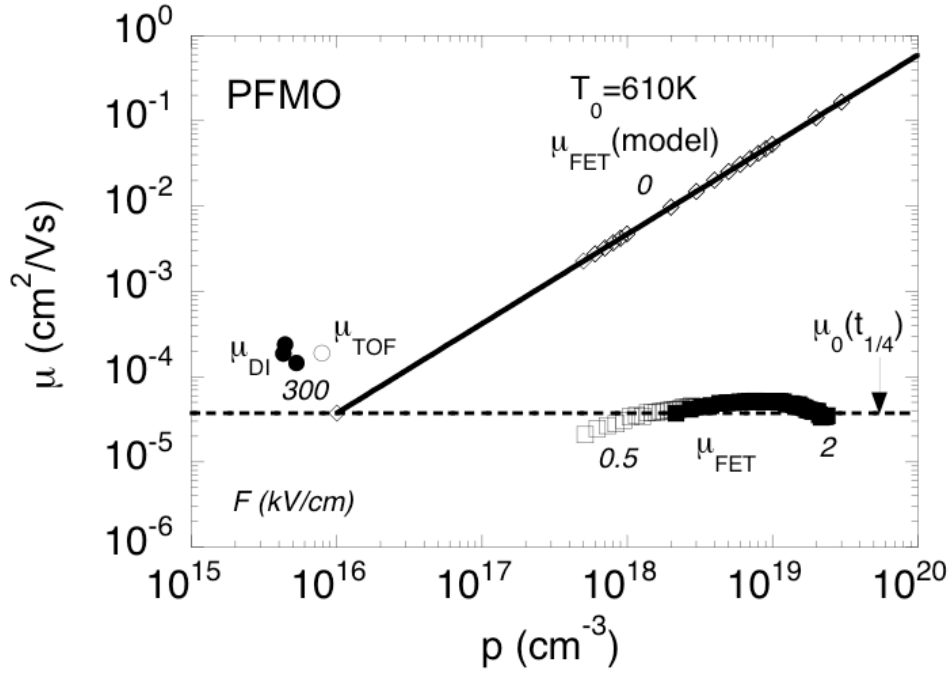

b)

Figure 5. Variation of the dark injection (DI), time-of-flight (TOF) and field-effect transistor (FET) hole mobility μ with charge-carrier density p for a) PFB and b) PFMO. Numerical values in italics indicate the applied field F in kV/cm. Horizontal dashed lines, equal to the zero-field TOF mobility $\mu_0(t_{1/4})$, are for a p-independent FET mobility. Solid lines and μ_{FET}*(model)* are for the p-dependent FET mobility model (at zero-field) in [5]. DI and TOF hole mobility values are taken from references [39-41].